Polarization-Independent Second-Order Photonic Topological Corner States

Linlin Lei,[1] Shuyuan Xiao,[2,3] Wenxing Liu,[1] Qinghua Liao,[1,*] Lingjuan He,[1] and Tianbao Yu[1,†]

[1] *School of Physics and Materials Science, Nanchang University, Nanchang, 330031, China*

[2] *Institute for Advanced Study, Nanchang University, Nanchang, 330031, China*

[3] *Jiangxi Key Laboratory for Microscale Interdisciplinary Study, Nanchang University, Nanchang, 330031, China*

(Received 26 June 2023; accepted 21 July 2023; published 4 August 2023)

Recently, much attention has been paid to second-order photonic topological insulators (SPTIs), because of their support for highly localized corner states with excellent robustness. SPTIs have been implemented in either transverse-magnetic (TM) or transverse-electric (TE) polarizations in two-dimensional photonic crystals (PCs), and the resultant topological corner states are polarization dependent, which limits their application in polarization-independent optics. However, to achieve polarization-independent corner states is not easy, since they are usually in-gap and the exact location in the topological band gap is not known in advance. Here we report on an SPTI based on a two-dimensional square-lattice PC made of an elliptic metamaterial, and we report that whether the band gap is topological or trivial depends on the choice of the unit cell. It is found that locations of topological band gaps of TM and TE polarizations in the frequency spectrum can be independently controlled by the out-of-plane permittivity $\varepsilon_\perp$ and the in-plane permittivity $\varepsilon_\parallel$, respectively, and more importantly, the location of in-gap corner states can also be separately manipulated by them. From this, we achieve topological corner states for both TM and TE polarizations with the same frequency in the PC by adjusting $\varepsilon_\perp$ and $\varepsilon_\parallel$, and their robustness with regard to disorders and defects is numerically demonstrated. The proposed SPTI provides a potential application scenario for polarization-independent topological photonic devices.

DOI: 10.1103/PhysRevApplied.20.024014

I. INTRODUCTION

Recently, the concept of higher-order topological insulators has been extended from electronic waves to classic waves [1–12]. It has been shown that higher-order topological insulators do not obey the usual bulk-edge correspondence but comply with the bulk-edge-corner correspondence [13–15]. For instance, a two-dimensional (2D) second-order topological insulator possesses one-dimensional gapped edge states and zero-dimensional in-gap corner states. In addition to the characteristics of strong field localization and small mode volume, zero-dimensional corner states also show excellent robustness with regard to fabrication flaws [16–18]. On this basis, they have enormous application value in the topological cavity [18,19], lasing [20,21], nonlinear optics [22,23], and sensing [24]. However, for photonic crystals (PCs), the two kinds of polarization, transverse-magnetic (TM) and transverse-electric (TE) modes, are usually studied in a separate way. One reason is either of the modes can be excited independently, each with its own band structure, and the other is that forming a common band gap (CBG) is not easy, especially the topological one. Research has shown the polarization-independent optics is potentially useful in polarization-independent waveguides relying on full band gaps [25], enhanced nonlinear optical effects [26], and polarization-division multiplexing [27]. Topologically protected polarization-independent optics would give them additional resistance to perturbation. It is worth noting that dual-polarization second-order photonic topological states were proposed by Huang *et al.* [28] recently on the basis of a topologically optimized geometric structure within a square lattice. However, the eigenfrequencies of topological states for the two polarizations are not the same, despite their having a common topological band gap.

In this paper, a 2D second-order photonic topological insulator (SPTI) is proposed, of which the topological states are polarization independent. The square-lattice PC, having a fishnet structure, is made of an elliptic metamaterial. The permittivity is anisotropic, and nevertheless the geometric structure is rather simple compared with the previously proposed topologically optimized structure. Whether the CBG is trivial or topological depends on the choice of the unit cell (UC) for the TM and TE modes. The proposed SPTI can host topological edge states and corner states for the two modes at the same time. Our results show polarization-independent topological corner

*lqhua@ncu.edu.cn

†yutianbao@ncu.edu.cn

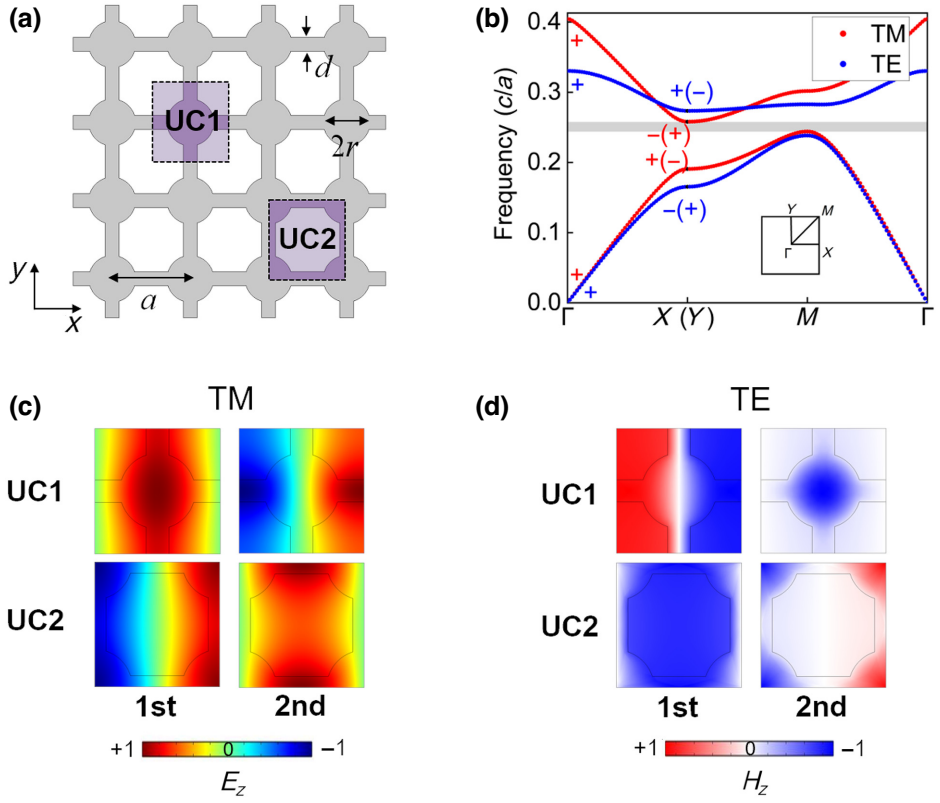

FIG. 1. (a) Fishnet PC and two kinds of UCs, UC1 and UC2. (b) Band structures of TM and TE modes, denoted by dotted red and blue, respectively. Even and odd parities of UC1 (UC2) at high-symmetry points are indicated by plus and minus signs, colored red and blue for TM and TE modes, respectively. (c) E_z patterns of the two TM bands at the X point for UC1 and UC2. (d) H_z patterns of the two TE bands at the X point for UC1 and UC2.

states based on an SPTI are not guaranteed by a common topological band gap. However, we find that the locations of the band gaps and corner states in the frequency spectrum can be manipulated independently by the out-of-plane permittivity $\varepsilon_\perp$ and the in-plane permittivity $\varepsilon_\parallel$ for the TM and TE modes, respectively, which gives an effective way to achieve overlapped corner states for the two modes. On this basis, corner states independent of polarization can be realized by our choosing appropriate $\varepsilon_\perp$ and $\varepsilon_\parallel$. Numerical simulations further show the corner states are topologically protected, with strong robustness with regard to disorders and defects. Our work shows potential applications in polarization-independent topological photonic devices.

II. STRUCTURE DESIGN AND BAND TOPOLOGY

For PCs, TM band gaps are favored in dielectric rods, while TE band gaps are favored in dielectric veins [29]. From this, the proposed square-lattice PC is constructed by thin dielectric veins with dielectric rods located at lattice sites, as shown in Fig. 1(a), where a is the lattice constant, and the circle radius r and vein width d are $0.3a$ and $0.18a$, respectively. The dielectric material is anisotropic, an elliptic metamaterial with permittivity $\varepsilon = (\varepsilon_\parallel, \varepsilon_\parallel, \varepsilon_\perp) = (16.9, 16.9, 10)$. Generally, topological corner states lie in a topological band gap [13], and hence a topological CBG of TM and TE polarizations is the prerequisite for polarization-independent topological corner states. The choice of the elliptic metamaterial is based on the consideration that the band-gap locations of TM and TE polarizations in the frequency spectrum can be manipulated independently by $\varepsilon_\perp$ and $\varepsilon_\parallel$, respectively. In practice, we can use the multilayer model to construct the anisotropic permittivity [30]. The multilayer consists of two alternate dielectrics with high and low permittivity, and it is placed horizontally in the x-y plane. According to the formulisms (16) and (17) proposed in Ref. [31], the PC slab with permittivity (16.9,16.9,10) can be approximately built with the high dielectric with permittivity of 17.67 and the air layer when the filling ratio of the high dielectric is 0.954. Herein, the calculation of band structures and the numerical simulations are based on the finite-element method and use of COMSOL MULTIPHYSICS.

UCs of two kinds based on the common square lattice, UC1 and UC2, are selected in Fig. 1(a). Note that the two

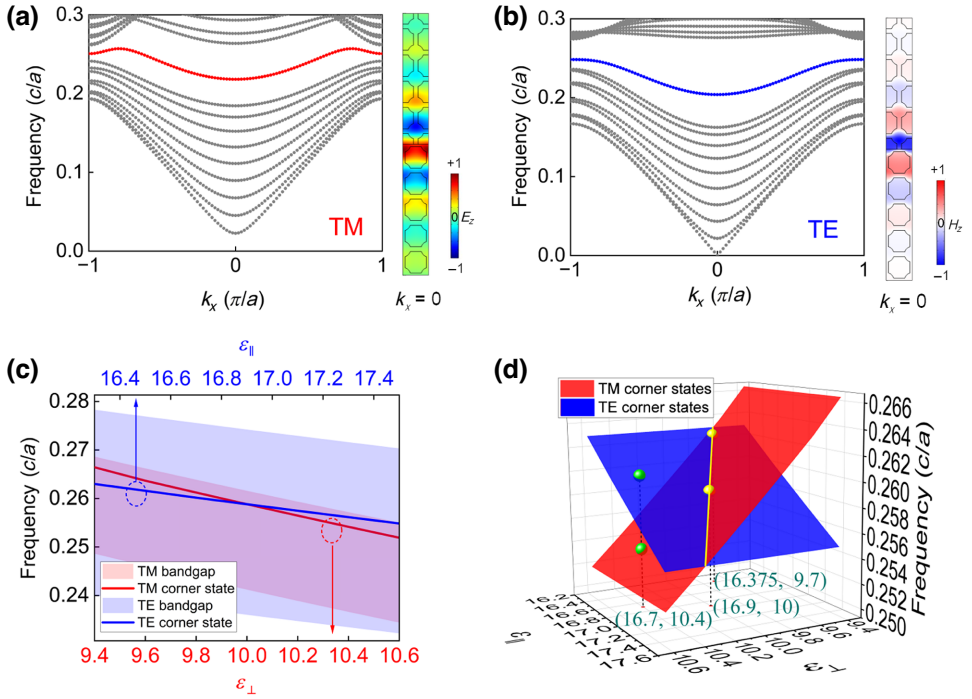

FIG. 2. Supercell band structures of (a) TM and (b) TE modes, with edge modes colored red and blue, respectively. Eigenfields at $k_x = 0$ show the edge modes can be well confined at the interface between UC1s and UC2s for the TM and TE modes. (c) Dependence of band gaps and eigenfrequencies of one of the corner states on $\varepsilon_\perp$ and $\varepsilon_\parallel$ for the two modes. The area shaded in light red indicates TM band gaps, while the area shaded in light blue indicates TE band gaps. The red and blue lines denote one of the corner states of TM and TE modes, respectively. (d) TM corner states (colored red) and TE corner states (colored blue) for any combination of $\varepsilon_\perp$ and $\varepsilon_\parallel$ in the same parameter range as for (c). The yellow intersecting line denotes the combinations that have overlapped corner states. The yellow points on the intersecting line are two of the combinations, and their anisotropic permittivities $(\varepsilon_\parallel, \varepsilon_\parallel, \varepsilon_\perp)$ are (16.9,16.9,10) and (16.375,16.375,9.7), respectively. The green points are the two points that share the same anisotropic permittivity (16.7,16.7,10.4) but have different eigenfrequencies.

UCs are consistent with each other after the center of one of the UCs has been shifted by half the period along the x and y directions. Therefore, they share the same band structure as plotted in Fig. 1(b), with dotted red and blue lines denoting the TM and TE modes, respectively. One can find that there is a CBG indicated by the gray region lying between the first and second bands of TM modes. However, for the two UCs, the CBG possesses different topological behaviors characterized by the 2D Zak phase (see Appendix A), which has the following form [32–34]:

$$\theta_j^{\mathrm{Zak}} = \int dk_x dk_y \mathrm{Tr}[\hat{A}_j(k_x, k_y)], \tag{1}$$

where $j = x$ or y, and the Berry connection $\hat{A}_j = i\langle u(\mathbf{k})|\nabla_{k_j}|u(\mathbf{k})\rangle$, with $u(\mathbf{k})$ being the periodic part of the Bloch function. The 2D Zak phase can also be understood by the 2D bulk polarization via $\theta_j^{\mathrm{Zak}} = 2\pi P_j$, with

$$P_j = \frac{1}{2}\left(\sum_n q_j^n \bmod 2\right), \qquad (-1)^{q_j^n} = \frac{\eta(X_j)}{\eta(\Gamma)}, \tag{2}$$

where P_j is determined by the parity η associated with π rotation at the Γ and X (Y) points and the summation is over all the occupied bands below the band gap. Here P_x is equal to P_y, namely, $P_x = P_y$, due to the C_4 symmetry [35,36]. Eigenfield patterns at the X point of the two bands for TM and TE modes are shown in Figs. 1(c) and 1(d), respectively, with the monopole having even parity and the dipole having odd parity. As can be seen, the parities of the two bands at the X point have an inversion between UC1 and UC2 for both modes, whereas the parities at the Γ point stay the same. Moreover, the parities of the same UC at the X point are opposite for the TM and TE modes, which gives the same UC distinct topological properties for the two modes. Concretely, for TM modes, the same parties of UC1 at the X and Γ points give the 2D bulk polarization (P_x, P_y) a value of $(0, 0)$ and the 2D Zak phase $(\theta_x^{\mathrm{Zak}}, \theta_y^{\mathrm{Zak}})$ a value of $(0, 0)$, while the distinct parity of UC2 at the X and Γ points makes $(P_x, P_y) = (\frac{1}{2}, \frac{1}{2})$ and $(\theta_x^{\mathrm{Zak}}, \theta_y^{\mathrm{Zak}}) = (\pi, \pi)$. The opposite is true for the TE modes. As a result, the band gap of UC1 is trivial and that of UC2 is topological for TM modes, and vice versa for TE modes.

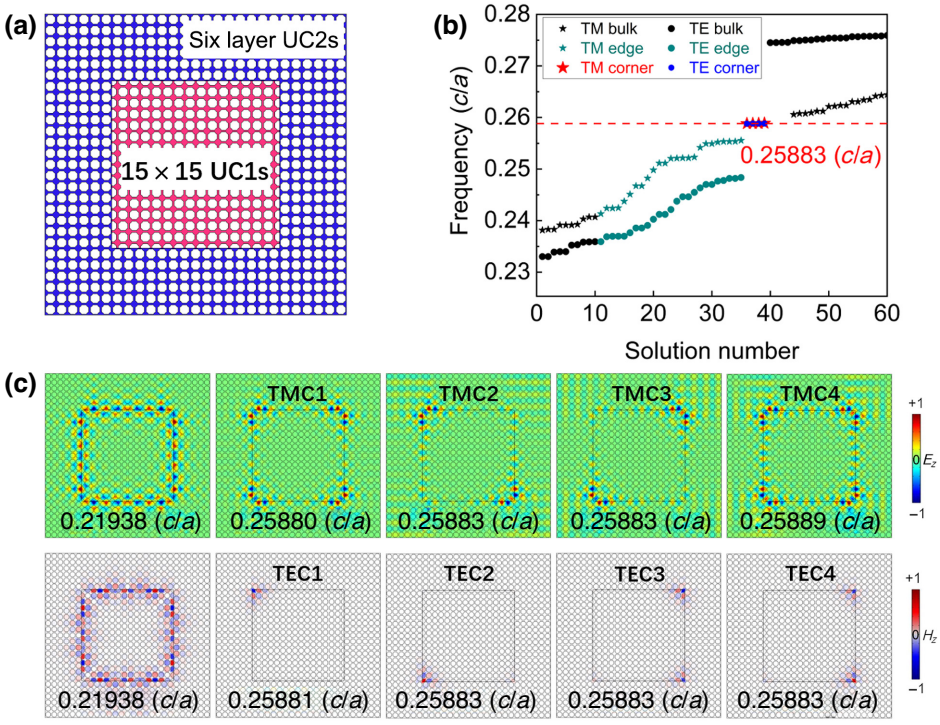

FIG. 3. (a) The finite-sized box-shaped PC, with 15 × 15 UC1s surrounded by six-layer UC2s. (b) Eigenfrequencies of the box-shaped PC. TM and TE modes are denoted by pentagons and circles, with their corner states colored red and blue, respectively. Edge modes are shown in cyan. (c) Eigenfields of the overlapped whispering-gallery modes and corner modes. TMC and TEC denote the TM and TE corner states, respectively.

III. POLARIZATION-INDEPENDENT TOPOLOGICAL CORNER STATES

The topological distinction between UC1 and UC2 ensures the existence of topological edge states [21,37–39]. To show this, we construct a supercell composed of five UC1s and five UC2s along the y direction; the band structures are shown in Figs. 2(a) and 2(b) for TM and TE modes, respectively. In the calculation, periodic boundary conditions and perfect-electric-conductor boundary conditions are applied to the x and y directions, respectively. As can be seen, there is one in-gap edge state for both modes, which does not occupy the whole bulk band gap and can be confined at the interface between UC1s and UC2s. Since the PC has C_4 symmetry, we can define a corner topological index: $Q^c = 1/4([X_1] + 2[M_1] + 3[M_2])$, where $[\Pi_p] = \#\Pi_p - \#\Gamma_p$, where Π stand for high symmetric

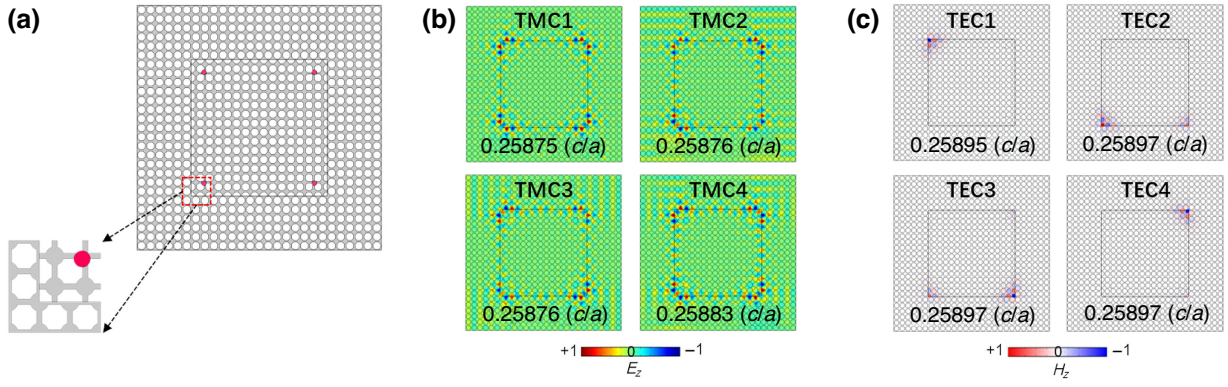

FIG. 4. (a) Box-shaped PC with four disorders (red dots) around four corners of the internal PC composed of UC1s. The enlarged view shows one of the four disorders, with a 10% decrease in the radius and a deviation of $0.1a$ from the lattice site along the x and y directions. Eigenfields of four corner modes of (b) TM and (c) TE modes under the influence of the disorders.

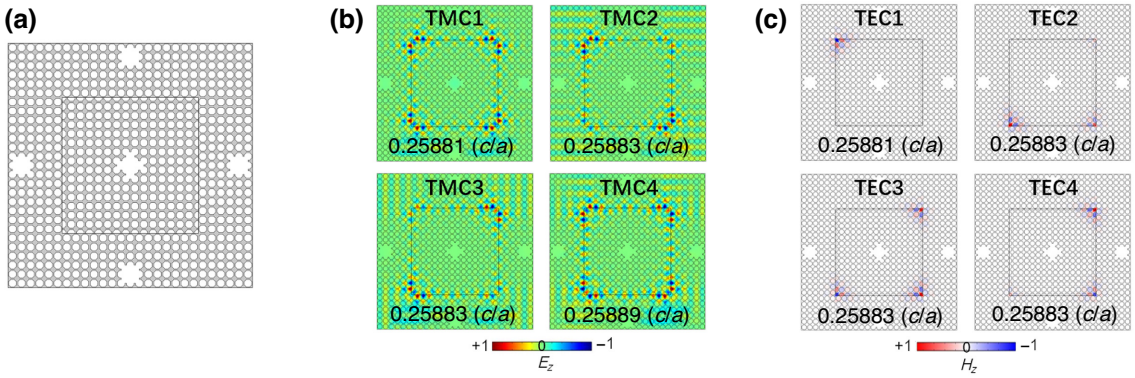

FIG. 5. (a) Box-shaped PC with defects produced by removal of five UC1s in the center and four UC2s near the edge of the PC. Eigenfields of four corner modes of (b) TM and (c) TE modes under the influence of the defects.

points X, M, and Γ, and $\#\Pi_p$ is defined as the number of bands below the band gap with rotation eigenvalues $\Pi_p^n = e^{[2\pi i(p-1)/n]}$ for $p = 1, 2, 3, 4$. The nontrivial TM and TE cases both have $[X_1] = -1$, $[M_1] = 1$, and $[M_2] = 0$. Therefore, the corner topological index is $Q^c = 1/4$ for both modes, indicating $1/4$ fractionalized corner states at each of the four corners [39].

It is noteworthy that the existence of polarization-independent corner states is not guaranteed by the CBG. In Fig. 2(c), we change $\varepsilon_\perp$ and $\varepsilon_\parallel$ in a certain range near (16.9, 16.9, 10) to solely adjust the positions of supercell band gaps in the frequency spectrum for TM and TE modes, respectively. Specifically, for the TM band gap, we increase $\varepsilon_\perp$ from 9.4 to 10.6 and keep $\varepsilon_\parallel$ at any value, while for the TE band gap, we increase $\varepsilon_\parallel$ from 16.3 to 17.5 and keep $\varepsilon_\perp$ at an arbitrary value. As can be seen, the positions of the two band gaps descend as the corresponding permittivity increases, and the TM band gap (light-red area) is completely embedded in the TE band gap (light-blue area), forming the CBG. We also calculate the eigenfrequencies of TM (red line) and TE (blue line) corner states from the finite-sized box-shaped PC shown in Fig. 3(a) using a 2D model with scattering boundary conditions applying to the boundaries of the PC, and find that they are in the CBG and the variation trend of the corner states with the permittivity is the same as that of the band gaps. Since the two kinds of polarized corner state are independent of each other, to search for the overlapped ones, we plot their eigenfrequencies under any combination of $\varepsilon_\perp$ and $\varepsilon_\parallel$ in Fig. 2(d). It can be observed that corner states of the two modes do not coincide with each other except on the yellow intersecting line. The yellow points on the intersecting line are two of the combinations that have the overlapped corner states, and the corresponding anisotropic permittivities $(\varepsilon_\parallel, \varepsilon_\parallel, \varepsilon_\perp)$ are (16.9,16.9,10) and (16.375,16.375,9.7). As a contrast, green points are the two points that share the same anisotropic permittivity (16.7,16.7,10.4) but have different eigenfrequencies. Therefore, the anisotropic permittivity provides an additional freedom to manipulate the location of corner states of the two modes, making the corner states either polarization independent or polarization separable (see Appendix B).

To verify the existence of the polarization-independent corner states, a box-shaped PC of finite size is constructed, which is composed of 15×15 UC1s surrounded by six-layer UC2s, as shown in Fig. 3(a). The calculated eigenfrequencies of TM and TE modes based on the anisotropic permittivity (16.9,16.9,10) are shown in Fig. 3(b). As can be seen, both show gapped edge modes and four in-gap corner modes. Dotted red and blue lines go through the overlapped corner and edge states, respectively. In Fig. 3(c), eigenfields of these topological states indicate that the edge modes can be well confined along the whole interface between UC1s and UC2s, while the corner states are highly localized at the corners of the internal PC formed by the UC1s. Remarkably, not only the whispering-gallery modes but also the topological corner states for the two modes share the same eigenfrequencies,, and their common eigenfrequency are 0.21938 (c/a) and 0.25883 (c/a), respectively. This is different from the previously reported dual-polarization topological corner states, which possess a topological CBG, but their eigenfrequencies are not overlapped at all [28].

The polarization-independent photonic corner states are topologically protected due to their topological origin [40,41]. To verify this, we introduce four disorders marked by red dots around the four corners into the perfect PC, as shown in Fig. 4(a). The enlarged view in Fig. 4(a) shows the single disorder, with a 10% decrease in the radius and a deviation of $0.1a$ from the lattice site along the x and y directions. Eigenfields of the corner states of TM and TE modes are shown in Figs. 4(b) and 4(c), respectively, from which we can see that the corner states still exist with negligible offsets of the eigenfrequencies. Beyond that, defects, produced by removal of five UC1s and four UC2s in the center and near the edge of the PC, respectively, are also introduced, as shown in Fig. 5(a). As can be seen in Figs. 5(b) and 5(c), since the defects are far away

from the corners, the eigenfrequencies of the corner states for the TM and TE modes remain unchanged, although the defects have a more-destructive effect on the PC structure [42].

IV. CONCLUSION

In summary, a polarization-independent SPTI based on a 2D square-lattice PC is achieved. The dielectric is an elliptic metamaterial, and the geometric structure is rather simple nevertheless. By selection of appropriate geometric parameters and anisotropic permittivity, a CBG is obtained for TM and TE modes. Whether the CBG of a certain UC is either trivial or topological depends on the polarization modes. Topological corner states of TM and TE modes can coexist in the CBG, but only the combinations of in-plane permittivity $\varepsilon_{\parallel}$ and out-of-plane permittivity $\varepsilon_{\perp}$ that lie on the intersecting line in the eigenfrequency-permittivity space can make them overlap. Numerical simulations further show they have strong robustness with regard to disorders and defects. The proposed scheme can be extended to corner states induced by the quadrupole topological phase in square lattices and to pseudospin and valley-spin degrees of freedom. Our work could pave the way toward designing high-performance polarization-independent topological photonic devices, such as a polarization-independent topological laser and a coupled cavity waveguide.

ACKNOWLEDGMENTS

The work was jointly supported by the National Natural Science Foundation of China (Grants No. 12064025 and No. 12264028), the Natural Science Foundation of Jiangxi Province (Grant No. 20212ACB202006), and the Open Project of the Education Ministry Key Laboratory of Radar Imaging and Microwave Photonic Technology.

APPENDIX A: TIGHT-BINDING MODEL

The tight-binding model describes well the topological phase transition between UC1 and UC2, in which one can take the dielectric rods as lattice sites for TM modes, while the air holes act the part for TE modes. The Hamiltonian has the following form:

$$H = -\sum_{ij} t_{ij} c_i^{\dagger} c_j, \tag{A1}$$

where t_{ij} is the hopping amplitude between the nearest lattice sites, $c_i^{\dagger}$ is the creation operator, and c_j is the annihilation operator. As there is only one lattice site in UCs, the band below the photonic band gap can be expressed as

$$\begin{aligned} E &= -t_0(e^{ik_x} + e^{-ik_x} + e^{ik_y} + e^{-ik_y}) \\ &= -2t_0(\cos k_x + \cos k_y). \end{aligned} \tag{A2}$$

For TM modes, for UC1, the lattice site chosen as the inversion center is at the center of UC1, and the inversion operator $I = 1$. Hence, the parities at the Γ and X points are the same. For UC2, the lattice sites are at the four corners and the inversion operator $I = e^{\pm i(k_x + k_y)}$ depends on which lattice site is referenced. Thus, the parity is $+1$ at the $\Gamma = (0, 0)$ point, while it is -1 at the $X = (\pi, 0)$ point [34].

For TE modes, the lattice sites of UC1 chosen as the inversion center are at the four corners, since the air holes instead of the dielectric rods play the role of lattice sites. For UC2, the lattice site chosen as the inversion center is at the center of UC2. As a consequence, the parities at the Γ and X points are opposite for UC1, while they are the same for UC2. The results are consistent with the parities shown in Fig. 1(b).

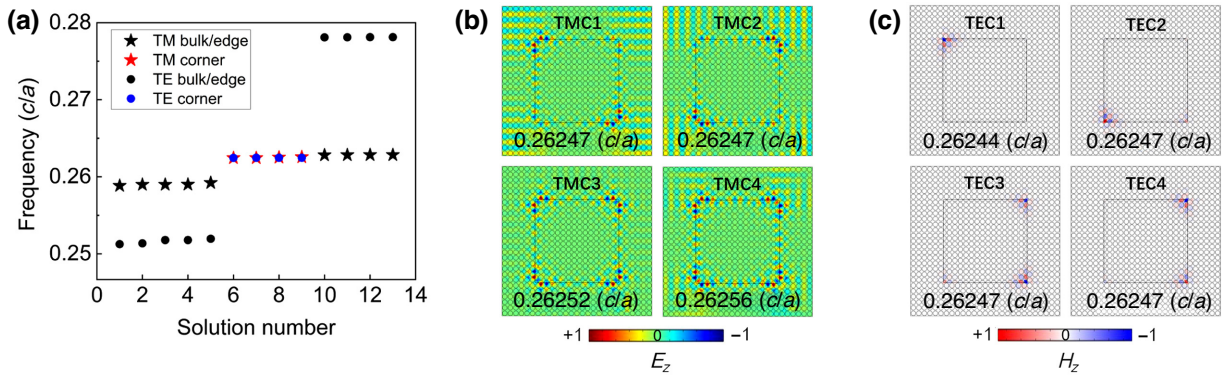

FIG. 6. (a) Eigenfrequencies of the box-shaped PC with an anisotropic permittivity of (16.375,16.375,9.7), showing overlapped corner states of TM and TE modes. Pentagons and circles denote TM and TE modes, and their corner states are colored red and blue, respectively. (b) Eigenfields of the corner states of TM modes. (c) Eigenfields of the corner states of TE modes.

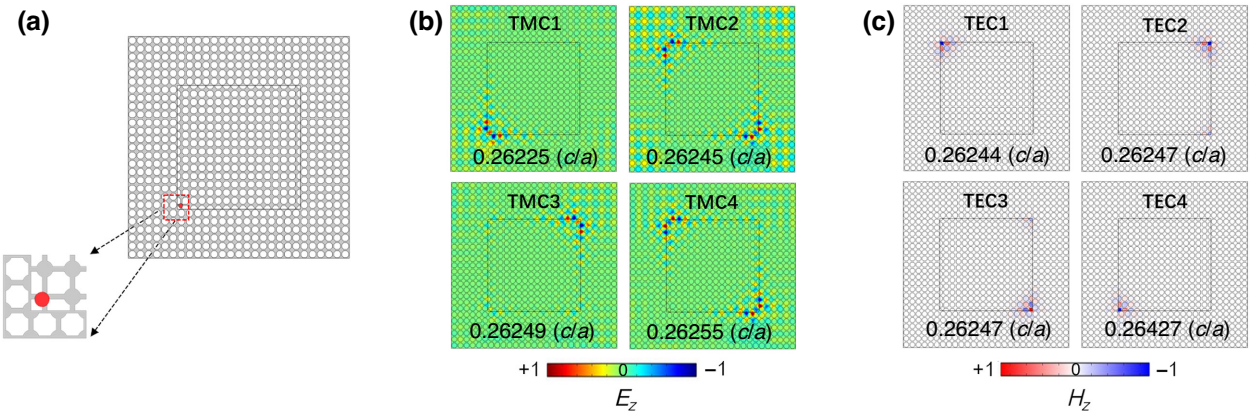

FIG. 7. (a) Box-shaped PC with a disorder (red dot) located at the bottom-left corner of the internal PC composed of UC1s. The enlarged view shows the single disorder, with a 10% decrease in the radius and a deviation of $0.1a$ from the lattice site along the x and y directions. Eigenfields of four corner modes of (b) TM and (c) TE modes under the influence of the disorder.

APPENDIX B: SWITCH BETWEEN POLARIZATION-INDEPENDENT AND POLARIZATION-SEPARABLE CORNER STATES

Here we show another anisotropic permittivity lying on the intersecting line that can achieve polarization-independent topological corner states. The anisotropic permittivity is (16.375, 16.375, 9.7), as indicated in Fig. 2(d). Figure 6(a) shows the calculated eigenfrequencies, from which we can see that the corner states of the two modes can be overlapped for this permittivity. Eigenfrequencies and eigenfields of the corner states are shown in Figs. 6(b) and 6(c), and one can see the overlapped eigenfrequency is 0.26247 (c/a). In Fig. 7, if we introduce a single disorder into the box-shaped PC, the corner states still survive with little frequency shift, but monopoles and quadrupoles of TM modes no longer exist due to the breaking of the C_4 symmetry of the box-shaped PC.

If the anisotropic permittivity is off the intersecting line, polarization-independent corner states will be changed into polarization-separable corner states. As shown in Fig. 2(d), if the anisotropic permittivity is (16.7,16.7,10.4), the eigenfrequencies of the corner states of the two modes are apart from each other. In detail, we plot the eigenfrequencies in Fig. 8(a), and one can see that none of the four corner states of the two modes is the same, and the maximum frequency difference between the two modes is 0.00606 (c/a) as shown in Figs. 8(b) and 8(c).

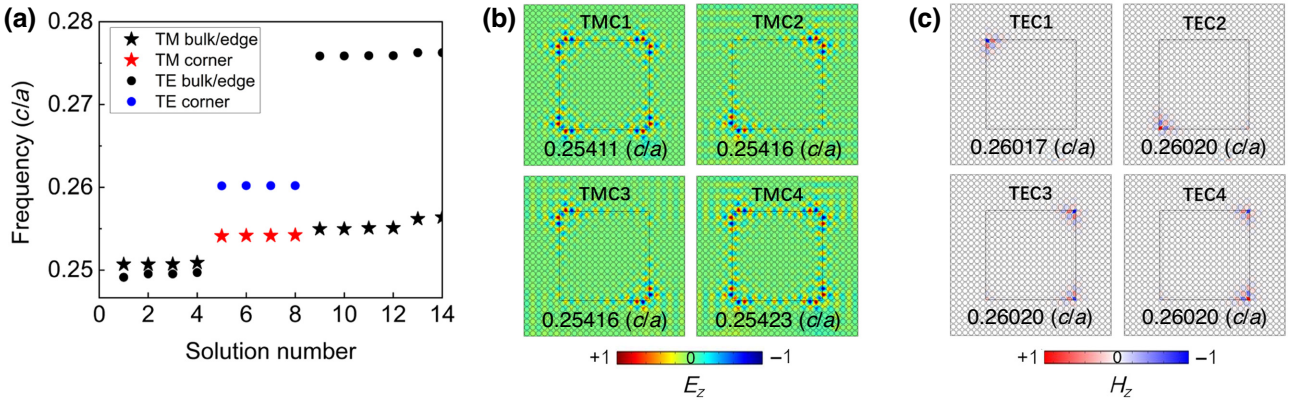

FIG. 8. (a) Eigenfrequencies of the box-shaped PC with an anisotropic permittivity of (16.7,16.7,10.4), showing corner states of TM and TE modes are not overlapped. Pentagons and circles denote TM and TE modes, and their corner states are colored red and blue, respectively. (b) Eigenfields of the corner states of TM modes. (c) Eigenfields of the corner states of TE modes.

[1] C. W. Peterson, W. A. Benalcazar, T. L. Hughes, and G. Bahl, A quantized microwave quadrupole insulator with topologically protected corner states, Nature **555**, 346 (2018).

[2] H. R. Xue, Y. H. Yang, F. Gao, Y. D. Chong, and B. L. Zhang, Acoustic higher-order topological insulator on a kagome lattice, Nat. Mater. **18**, 108 (2019).

[3] S. Y. Huo, H. B. Huang, L. Y. Feng, and J. J. Chen, Edge states and corner modes in second-order topological phononic crystal plates, Appl. Phys. Express **12**, 094003 (2019).

[4] Y. T. Yang, Z. Y. Jia, Y. J. Wu, R. C. Xiao, Z. H. Hang, H. Jiang, and X. Xie, Gapped topological kink states and topological corner states in honeycomb lattice, Sci. Bull. **65**, 531 (2020).

[5] Z. Z. Yang, X. Li, Y. Y. Peng, X. Y. Zou, and J. C. Cheng, Helical Higher-Order Topological States in an Acoustic Crystalline Insulator, Phys. Rev. Lett. **125**, 255502 (2020).

[6] H. M. Mu, B. Liu, T. Y. Hu, and Z. F. Wang, Kekulé lattice in graphdiyne: Coexistence of phononic and electronic second-order topological insulator, Nano Lett. **22**, 1122 (2022).

[7] S. G. Marc, V. Peri, R. Süsstrunk, R. B. Osama, L. Tom, L. G. Villanueva, and D. H. Sebastian, Observation of a phononic quadrupole topological insulator, Nature **555**, 342 (2018).

[8] X. Ni, M. Weiner, A. Alù, and A. B. Khanikaev, Observation of higher-order topological acoustic states protected by generalized chiral symmetry, Nat. Mater. **18**, 113 (2019).

[9] L. He, Z. Addison, E. J. Mele, and B. Zhen, Quadrupole topological photonic crystals, Nat. Commun. **11**, 3119 (2020).

[10] W. A. Benalcazar, B. A. Bernevig, and T. L. Hughes, Quantized electric multipole insulators, Science **357**, 61 (2017).

[11] S. W. An, T. Liu, H. Y. Fan, H. Gao, Z. M. Gu, S. J. Liang, S. B. Huang, Y. Zheng, Y. F. Chen, L. Cheng, and J. Zhu, Second-order elastic topological insulator with valley-selective corner states, Int. J. Mech. Sci. **224**, 107337 (2022).

[12] B. Y. Xie, H. F. Wang, H. X. Wang, X. Y. Zhu, J. H. Jiang, M. H. Lu, and Y. F. Chen, Second-order photonic topological insulator with corner states, Phys. Rev. B **98**, 205147 (2018).

[13] Z. G. Chen, C. Q. Xu, R. A. Jahdali, J. Mei, and Y. Wu, Corner states in a second-order acoustic topological insulator as bound states in the continuum, Phys. Rev. B **100**, 075120 (2019).

[14] M. Li, D. Zhirihin, M. Gorlach, X. Ni, D. Filonov, A. Slobozhanyuk, A. Alù, and A. B. Khanikaev, Higher-order topological states in photonic kagome crystals with long-range interactions, Nat. Photon. **14**, 89 (2020).

[15] X. Zhang, H.-X. Wang, Z.-K. Lin, Y. Tian, B. Xie, M.-H. Lu, Y.-F. Chen, and J.-H. Jiang, Second-order topology and multidimensional topological transitions in sonic crystals, Nat. Phys. **15**, 582 (2019).

[16] A. Q. Shi, B. Yan, R. Ge, J. L. Xie, Y. C. Peng, H. Li, W. E. I. Sha, and J. J. Liu, Coupled cavity-waveguide based on topological corner state and edge state, Opt. Lett. **46**, 1089 (2021).

[17] X. D. Chen, W. M. Deng, F. L. Shi, F. L. Zhao, M. Chen, and J. W. Dong, Direct Observation of Corner States in Second-Order Topological Photonic Crystal Slabs, Phys. Rev. Lett. **122**, 233902 (2019).

[18] O. Yasutomo, L. Feng, K. Ryota, W. Katsuyuki, W. Katsunori, A. Yasuhiko, and I. Satoshi, Photonic crystal nanocavity based on a topological corner state, Optica **6**, 786 (2019).

[19] X. Xie, W. Zhang, X. He, S. Wu, J. Dang, K. Peng, F. Song, L. Yang, H. Ni, Z. Niu, C. Wang, K. Jin, X. Zhang, and X. Xu, Cavity quantum electrodynamics with second-order topological corner state, Laser Photon. Rev. **14**, 1900425 (2020).

[20] H. R. Kim, M. S. Hwang, D. Smirnova, K. Y. Jeong, Y. Kivshar, and H. G. Park, Multipolar lasing modes from topological corner states, Nat. Commun. **11**, 5758 (2020).

[21] H. Zhong, Y. V. Kartashov, A. Szameit, Y. D. Li, C. L. Liu, and Y. Q. Zhang, Theory of topological corner state laser in kagome waveguide arrays, APL Photon. **6**, 040802 (2021).

[22] Z. Hu, D. Bongiovanni, D. Jukić, E. Jajtić, S. Xia, D. Song, J. Xu, R. Morandotti, H. Buljan, and Z. Chen, Nonlinear control of photonic higher-order topological bound states in the continuum, Light Sci. Appl. **10**, 164 (2021).

[23] S. S. Kruk, W. Gao, D.-Y. Choi, T. Zentgraf, S. Zhang, and Y. Kivshar, Nonlinear imaging of nanoscale topological corner states, Nano Lett. **21**, 4592 (2021).

[24] M. Chao, Q. Liu, W. Zhang, L. Zhuang, and G. Song, Mutual coupling of corner-localized quasi-BICs in high-order topological PhCs and sensing applications, Opt. Express **30**, 29258 (2022).

[25] H. Wu, D. S. Citrin, L. Y. Jiang, and X. Y. Li, Polarization-independent single-mode waveguiding with honeycomb photonic crystals, IEEE Photon. Technol. Lett. **27**, 840 (2015).

[26] Y. N. Zhang, W. M. Murray, B. B. Lan, and L. Marko, Ultra-high-Q TE/TM dual-polarized photonic crystal nanocavities, Opt. Lett. **34**, 2694 (2009).

[27] D. X. Dai and J. E. Bowers, Silicon-based on-chip multiplexing technologies and devices for peta-bit optical interconnects, Nanophotonics **3**, 283 (2014).

[28] Y. F. Chen, F. Meng, Z. H. Lan, B. H. Jia, and X. D. Huang, Dual-Polarization Second-Order Photonic Topological Insulators, Phys. Rev. Appl. **15**, 034053 (2021).

[29] Y. F. Chau, F. L. Wu, Z. H. Jiang, and H. Y. Li, Evolution of the complete photonic bandgap of two-dimensional photonic crystal, Opt. Express **19**, 4862 (2011).

[30] J. R. Wang, X. D. Chen, F. L. Zhao, and J. W. Dong, Full polarization conical dispersion and zero-refractive-index in two-dimensional photonic hypercrystals, Sci. Rep. **6**, 22739 (2016).

[31] L. Ferrari, C. Wu, D. Lepage, X. Zhang, and Z. Liu, Hyperbolic metamaterials and their applications, Prog. Quantum Electron. **40**, 1 (2015).

[32] Y. F. Chen, Z. H. Lan, and J. Zhu, Inversely Designed Second-Order Photonic Topological Insulator with Multiband Corner States, Phys. Rev. Appl. **17**, 054003 (2022).

[33] F. Liu and K. Wakabayashi, Novel Topological Phase with a Zero Berry Curvature, Phys. Rev. Lett. **118**, 076803 (2017).

[34] Y. F. Chen, Z. H. Lan, and J. Zhu, Second-order topological phases in C_{4v}-symmetric photonic crystals beyond the two-dimensional Su-Schrieffer–Heeger model, Nanophotonics **11**, 1345 (2022).

[35] X. T. He, M. Y. Li, H. Y. Qiu, W. S. Ruan, L. D. Zhou, L. Liu, X. D. Chen, W. J. Chen, F. L. Zhao, and J. W. Dong, In-plane excitation of a topological nanophotonic corner state at telecom wavelengths in a cross-coupled cavity, Photon. Res. **9**, 1423 (2021).

[36] Z. J. Zhang, J. B. Yang, T. Du, and X. P. Jiang, Topological multipolar corner state in a supercell metasurface and its interplay with two-dimensional materials, Photon. Res. **10**, 855 (2022).

[37] L. Liu, Y. K. Wang, F. X. Zheng, and T. Sang, Multimode interference in topological photonic heterostructure, Opt. Lett. **47**, 2634 (2022).

[38] G. C. Ma, M. Xiao, and C. T. Chan, Topological phases in acoustic and mechanical systems, Nat. Rev. Phys. **1**, 281 (2019).

[39] B. Y. Xie, G. X. Su, H. F. Wang, H. Su, X. P. Shen, P. Zhan, M. H. Lu, Z. L. Wang, and Y. F. Chen, Visualization of Higher-Order Topological Insulating Phases in Two-Dimensional Dielectric Photonic Crystals, Phys. Rev. Lett. **122**, 233903 (2019).

[40] M. Proctor, P. A. Huidobro, B. Bradlyn, M. B. de Paz, M. G. Vergniory, D. Bercioux, and A. García-Etxarri, Robustness of topological corner modes in photonic crystals, Phys. Rev. Res. **2**, 042038(R) (2020).

[41] S. Wu, B. Jiang, Y. Liu, and J.-H. Jiang, All-dielectric photonic crystal with unconventional higher-order topology, Photon. Res. **9**, 668 (2021).

[42] Z. W. Zhang, H. Y. Long, C. Liu, C. Shao, Y. Cheng, X. J. Liu, and J. Christensen, Deep-subwavelength holey acoustic second-order topological insulators, Adv. Mater. **31**, 1904682 (2019).